Petroleum and Coal

Article Open Access

Methane Decomposition on a Homemade Ni-Co Catalyst for an Environmentally Benign Production of H_2 and Carbon Nanotubes: Kinetic and Performance Study

Hiba A. Abdulkareem, Rafi J. Algawi, Mazin N. Abdullah

Department of Petroleum Processes, Tikrit University, Iraq

Received September 27, 2020; Revised October 16; Accepted December 21, 2020

Abstract

Despite the high purity hydrogen demand is ever-growing, the traditional reforming methods still lacking the technique needed for clean production. The use of the appropriate catalyst and adjusting the operating conditions is the key to generate energy with both high quality and rate of production. In the present work, the co-impregnation method was used to prepare alumina supported 8.5 %Ni-7% Co catalyst. The prepared catalyst was characterized by surface area, pore size, and metal dispersion. The catalyst was then evaluated against a commercial 15.5 % Ni supported on alumina for the decomposition of synthetic natural gas to CO_2/CO free hydrogen and carbon nanotubes. The metal catalytic decomposition was experimentally conducted in a flow fixed bed quartz reactor at different temperatures and atmospheric pressure. The kinetic model of the decomposition over the prepared catalyst was obtained. The results revealed that the prepared bimetallic 8.5 %Ni-7% Co catalyst exhibited obvious improvement in catalytic decomposition compared to the commercial catalyst. It was also proven that the deactivation rate of the prepared catalyst was satisfactory because of the influence of the nanotubes that promoted the catalytic decomposition into clean hydrogen.

Keywords: *COx free hydrogen; Ni-Co catalyst; Carbon nanotubes; Decomposition; Natural gas.*

1. Introduction

At present, hydrogen is considered as the high energy fuel as it releases the least exhaust gases such as COx (CO_2/CO). Several conventional processes were developed for the production of hydrogen, such as coal gasification [1-3], natural gas steam reforming [4-6], alcohol steam reforming [7-9], reforming of biomass [10-13], and electrolysis of water [14-17]. Steam reforming of natural gas and methanol are the dominant industrial processes for the production of hydrogen. However, the growing restrictions in the legislation about CO_2 emissions (the steam reforming process produces 6 ton CO_2 per ton of H_2 [18]) motivated numerous researchers to investigate and develop different technologies of clean production of hydrogen [19-24]. Although these technologies were well presented, there are still several limitations and challenges that must be solved, and requirements must be fulfilled to become commercial processes. Among the possible technologies to produce hydrogen, the moderately endothermic catalytic methane decomposition fulfills those requirements [25-26], as the methane decomposition process reduces the CO/CO_2 emissions, and produces CO_x free hydrogen according to equation 1:

$$CH_{4(g)} \rightarrow C + 2H_2 \,, \qquad \Delta H_{1073} = 90.1\, kJ/mol(CH_4) \qquad (1)$$

In equation 1, the carbon generated as a side-product represented a valuable product due to its unique microstructure (nanofibers or nanotubes may be generated). This nanostructure carbon has diverse applications nowadays in reinforced structures, fuel cells, and electrochemical catalysis [27]. Different elements were utilized in the catalytic systems used to produce hydrogen from methane, such as carbonaceous materials, noble elements (Pt, Pd, and Re), and group VIII transition metals. One of the key disadvantages of this process, nevertheless, is the deactivation and recovery of catalysts, which are significantly impeded by the large concentrations of encapsulated carbon produced during the process and accumulated on the catalyst surface and active sites [28]. It must be noted that in this case, carbon is not formed through undesired secondary reactions, but it is one of the two products of the main reaction shown in equation 1. Proceeding with extensive efforts to overcome this hindrance, it has been found that using a certain metal combination for the catalytic decomposition of methane resulted in the production of carbon nanofibers or carbon nanotubes rather than the encapsulated carbon [29-31]. It has been reported that nickel catalysts catalyze the methane decomposition reaction into hydrogen and carbon as C-nanofibers [32-33]. For the prevention of the formation of encapsulated carbon mild decomposition conditions must be used, in parallel, these conditions favor low H_2 rates and low conversion of the methane. Therefore, if the aim of the methane decomposition reaction is the H_2 production, the high conversion is pursued, and the metal catalysts must be stabilized to guarantee the stability of the active centers during the process. Deactivation represents a challenge to oppose methane conversion into hydrogen; however, the literature lacks a process to enhance the high rate of production of COx free hydrogen along with the formation of carbon nanotubes and expressing a model for the rate of deactivation over a metal combination catalyst (Ni-Co/alumina). Thus, the present study aims to studying the thermocatalytic decomposition (TCD) of methane at different conditions of temperature, initial concentrations, and time on stream over a modified homemade catalyst against a commercial catalyst and the deactivation kinetic of the process. Also, the study focuses on optimum conditions necessary to produce high quality carbon nanotubes.

2. Experimental

2.1. Catalyst preparation

In the present study, the Ni-Co/Al_2O_3 catalyst was prepared by an effective impregnation method. The chemicals used for the preparation were; nickel nitrate ($Ni(NO_3)_2.6H_2O$, 99% purity, Himedia, USA), cobalt nitrate $Co(NO_3)_2.6H_2O$, 99% purity, Alpha, USA), and gamma-alumina spherical particles with specifications shown in Table 1. The loading weights of the transition metals impregnated in the alumina were 7% Co and 8.5% Ni. To prepare the impregnation solution, 16 g of cobalt salt was dissolved with 19 g of nickel salt in deionized water in a magnetic heater stirrer (Jisico, Korea) for one hour at 42°C until obtaining a saturated solution. The solution was used to impregnate 100 g of γ- alumina particles. To activate the catalyst sites, 3% of the H_3PO_4 solution was added with controlling the pH of the impregnated sites by stirring for one hour at the same until the alumina were entirely impregnated. The impregnated alumina particles were dried overnight at 125℃, then calcined at 650℃ for four [34]. The commercial reforming catalyst used in this investigation was NG-610-6H, UNICAT Catalyst Technologies Inc. The properties of the commercial catalyst are shown in Table 2.

Table 1. Aluminum oxide (γ-Al_2O_3) specifications

Catalyst	γ-Al_2O_3	Surface area, m^2/g	289
Pore volume, cm^3/g	0.83	Particle diameter, mm	5
Bulk density, g/cm^3	0.95	Particle shape	Sphere

Table 2. Ni commercial specifications

Property	value	Property	value
Pore volume, cm^3/g	0.56	Particle shape	Sphere
Bulk density, g/cm^3	1.03	Ni %	15.53
Surface area, m^2/g	232	Al_2O_3	balance
Particle diameter, cm	0.8		

2.2. Textural characterization of the catalyst

The surface area is one of the most indicative properties of a catalyst, and it is a measure of the goodness of the preparation method. The surface area and pore size of the Ni-Co/alumina catalyst prepared in the present study was determined by Brunner Emmet Teller (BET) method. The apparatus used for this purpose is Sorptometric-1990 (CE Instruments, Italy). Liquid N_2

at the boiling point of -200°C was pressurized inside the pore of the catalyst at the time of the BET test. Before that, the pores were degassed at 380°C for ten hours. This test was conducted to calculate the specific surface area of the catalyst at mesopores condition that is the range of relative pressure was $0.04 < P/P_0 < 0.28$. Also, the pore size was determined using the adsorption and desorption of the liquid nitrogen at a relative pressure of 0.995. To examine the microstructure and quality of surface distribution of the active components, high vacuum FEI Scanning Electron Microscopy (SEM, Quanta 200 FESEM, Switzerland) was used.

2.3. Catalytic activity evaluation

The feedstock used in this study was synthetic natural gas composed of methane (99.999% purity, National Oxygen Ltd, India was used without further purification) and argon (99.998% purity, Bristol Gases, UAE was used without further purification).

The performances of the homemade and commercial catalysts were evaluated for thermo-catalytic decomposition (TCD) of methane in a flow fixed bed reactor. Three gas bottles of different gases are connected to the reactor, argon gas which is used for warming up, purging, cooling, and as the carrier of the methane gas; hydrogen gas which was used for the reduction of the metallic catalyst, since the methane gas can also reduce metals at elevated temperature and produce CO/CO_2 gases (that rarely happen in the presence of H_2 gas); and methane gas which is used as a feed to test the catalyst activity. Each of the three gases was connected to a calibrated rotameter. Before reaction, methane and argon were mixed to the desired ratio and fed to a preheater and brought to the desired temperature of TCD.

The preheater consists of an aluminum block with an electrical coil heater mounted. A thermocouple type J was attached in the middle way of the preheater, which was controlled by a temperature controller (GEMO temperature controller. DT109A, Gurbuzoglu Elektronik San. ve Tic. Ltd., Turkey). The maximum temperature offer by the controller is 1243 ºC. The hot gas mixture was fed to the TCD reactor. The reactor is a tubular reactor made of quartz, which was selected as a material of fabricating over stainless steel because the dry reforming is notorious for producing coke when performed over base metals. Also, quartz is a poor conductor of heat, which is desirable for an endothermic reforming reaction.

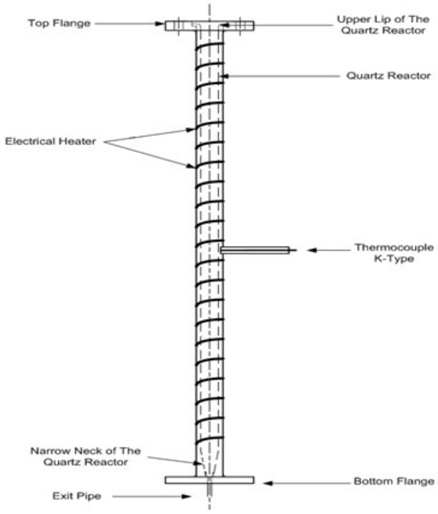

Figure 1. The TCD tubular reactor

The quartz tubular reactor was 15 mm internal diameter and 59 cm length with a wide neck up and narrow one down; the quartz tube was purchased with the surface quality of 10 and transmitted wavefront distortion of λ/10 at 62.8 nm. The quartz tube was housed by 316L stainless steel pipe fitted to a two modified 3/8″× 150 lbs flanges, a bottom flange with a longitude ring welded in 17mm diameter and 5mm height to prevent any leakage from the bottom of the reactor, and a top flange which was grooved in 2 mm depth and 21 mm diameter to fit the upper neck of the reactor, the schematic diagram of the reactor and the housing pipe is shown in Figure 1. The housing pipe is grooved, and a K-type thermocouple was installed in the middle of the housing pipe. An external electrical coil heater with ceramic beads, 3210-series furnace made by Applied Test System Inc., USA, was placed along the housing pipe to ensure a uniform distribution of heat. Inert ceramic balls were placed above and below the catalyst to keep the catalytic bed in the middle of the reactor.

The reactor was then wrapped with a layer of insulation to prevent heat loss. Two pressure gauges were placed before and after the reactor to adjust the pressure down the reactor as carbon deposited on the catalyst. The reactor was supplied with a cooling jacket to maintain the temperature of the exit stream below 50ºC which is recommended for the operation of the online hydrogen analyzer (K6050, Hitech Instruments, UK, 0.1% Accuracy: ±0.1% (5 to 100% of scale)). Then the product gases flowed through a filter with a trap supplied with a two-way exit valve; the first goes to the gas analyzer and the second to the vent. Figure 2 shows the experimental setup for the TCD process.

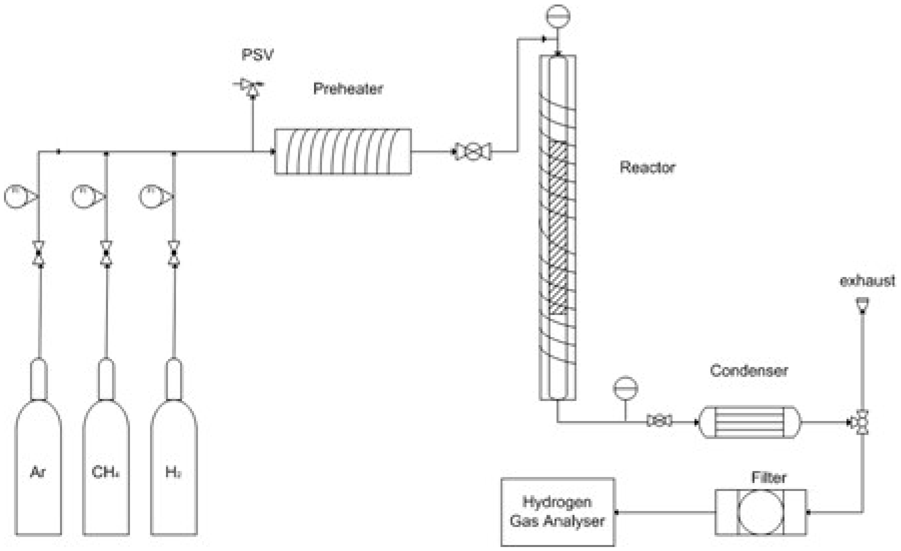

Figure 2. The experimental setup of the TCD process

Running of experiments were conducted as follow;

1. The catalyst was placed inside the reactor between the upper and lower ceramic balls.
2. The temperature controllers were turned on.
3. Argon gas was introduced at an 800mL/min for 20 min to warm up the reactor to 400ºC.
4. 100 mL/min of hydrogen gas was flowed to obtain 11% vol. gas mixture. The temperature was raised to 500ºC, which the reduction temperature of the prepared catalyst and to 550°C for the reduction of the commercial catalyst.
5. Turn on the cooling water to cool the outlet gas mixture.
6. Shut off the hydrogen reduction gas and starting the heating up of the reactor to the desired TCD temperature.
7. Feeding of methane gas along with the argon to obtain the desired mole fraction of methane.
8. The online hydrogen analyzer was turned on to read and record the concentration of hydrogen produced with time on stream up to 100 min.
9. Turning of methane gas value and the heater then purging with argon.
10. Turning of the cooling system and bringing the TCD unit to the safe shutdown state.

Table 3 summaries the operation variables studied in this investigation. In all experiments, a pressure of 1 atm was held constant.

Table 3. Operation variables of the present study

Parameter	Variables №s	Variables №s	Values
Catalyst	1	2	Homemade and commercial
Temperature, ºC	2	2	800, 900
Mole fraction of CH_4	5	5	0.6, 0.7, 0.8, 0.9, 1.0
Time on stream, min	1	1	Up to 60

2.4. Kinetics of TCD process

For the present newly developed TCD Ni-Co/alumina catalyst, it is important to analyze the kinetic of the TCD reaction over this catalyst to obtain the kinetic parameters. Determination of the apparent rate law of TCD using the prepared catalyst in the laboratory tubular reactor is the primary step to scale up to a commercial reactor. To obtain the rate expression of the

TCD reaction over the prepared catalyst, the integral method was used, and a guessed reaction order was assumed to test the experimental data. The following hypotheses were assumed for the TCD reaction in the tubular reactor:

- The tubular reactor is running at isothermal and isobaric steady-state conditions.
- The methane gas mixture is considered homogeneous to neglect the resistance of gas side mass transfer.
- Both feed and products of the TCD reaction are in the gas phase inside the reactor.
- The bed of the TCD reactor is narrow and short enough to ignore the axial and radial dispersion.
- The catalyst bed is completely wetted with the gas mixture; that is, the catalyst pores are filled with the gas mixture. Thus, the temperature gradient within the catalyst particles is neglected.
- Despite the TCD reaction, the physical properties of the gas mixture are constant.
- All the flow and mass transfer properties vary only with vertical location and time.

Usually, for catalyst testing at a laboratory scale and to obtain intrinsic parameters of any rate of reaction, kinetic models can be used. Assume *n-th* order kinetics for the chemical complexity of the reaction.

$$-r_{CH_4} = -\frac{dC_{CH_4}}{dt} = K_{app}C_{CH_4}^{n} \tag{2}$$

where K_{app}= apparent reaction rate constant ; C_{CH_4}= concentration of CH_4 at any time of the reaction.

The reaction rate is constant for TCD reaction K_{app} can be determined for each reaction using the modified Arrhenius equation as follows:

Arrhenius equation:

$$K_{app} = K_0 e^{-\frac{E_A}{RT}} \tag{3}$$

In equation 2, K_o is the pre-exponential factor or frequency factor; E_A is the apparent activation energy of the reaction; R is the gas constant, and T is the absolute temperature.

$$\text{In } K_{app} = -\frac{E_A}{R}\frac{1}{T} + lnK_0 \tag{4}$$

$$-r_{CH_4} = -\frac{dC_{CH_4}}{dt} = K_0 e^{-\frac{E_A}{RT}}\, C_{CH_4}^{n}$$

$$-r_{CH_4} = -\frac{dC_{CH_4}}{dt} = K_{app}C_{CH_4}^{n} \tag{5}$$

$$C_{CH_4} = \frac{c_{CH_40}(1-X)}{1+\epsilon X}, \epsilon = 2-1 = 1, \frac{d}{dt}\left(\frac{1-X}{1+X}\right) = K_{app}\frac{c_{CH_40}(1-X)^{n}}{1+\epsilon X}$$

Thus, least square method will be used to solve for the kinetic parameters *Kapp* and n constants in equation 5.

$$\frac{d}{dt}\left(\frac{1-X}{1+X}\right) = K_{app}\frac{(1-X)^{n}}{1+\epsilon X} \tag{6}$$

3. Results and discussion

3.1. Characterization of the homemade catalyst

The microstructure of the homemade Ni-Co on alumina TCD catalyst is shown in Figure 3. It is evident that metal particles were well dispersed within the texture of alumina particles. This indicates that the impregnation method of preparation was satisfactory to obtain a good dispersion of Mo and Co oxides over the alumina support. It is also shown that there were no clusters or agglomerates of metal particles throughout the support that is increasing the TCD catalyst activity.

The BET isotherms, and the pore volume profiles of the Ni-Co/ γ-Al_2O_3 catalyst are shown in Figure 4. Compared to the standard N_2 absorption-desorption curves, it can be seen that the isotherms of the homemade catalyst follow type IV isotherm, i.e. the catalyst is capable of surface adsorption. Also, the cycle of adsorption-desorption was obtained relative pressure range of $0.2<P/P_0 < 0.6$ revealing a mesopore structure with a pore volume of 0.62 cm³/g. The BET surface area obtained is 224 m²/g, which is still higher than the commercial catalyst (232 m²/g). These results depicted a well-designed Ni-Co catalyst.

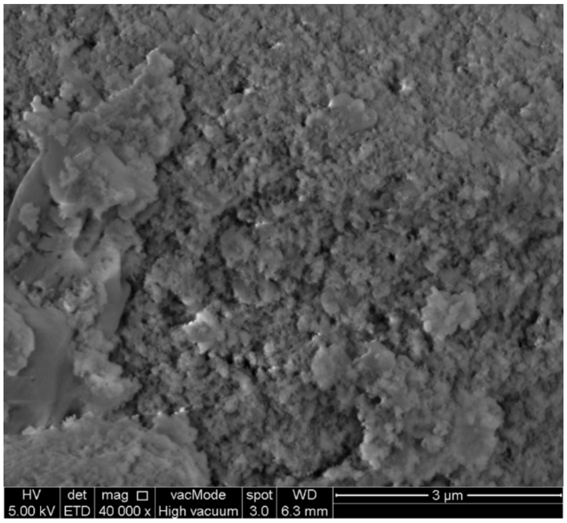

Figure 3a. SEM images of the Ni-Co/alumina homemade catalyst

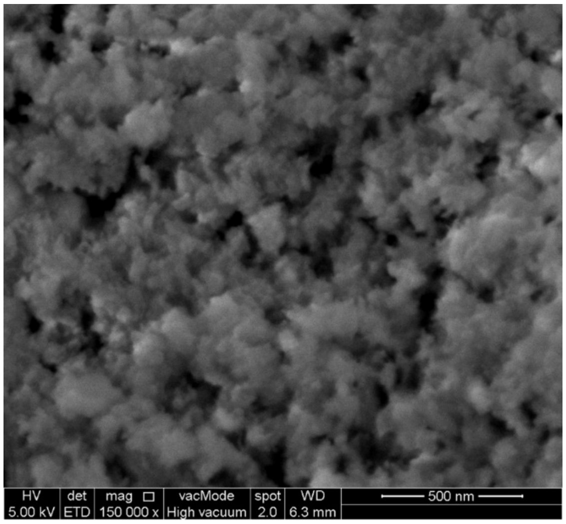

Figure 3b. SEM images of the Ni-Co/alumina homemade catalyst

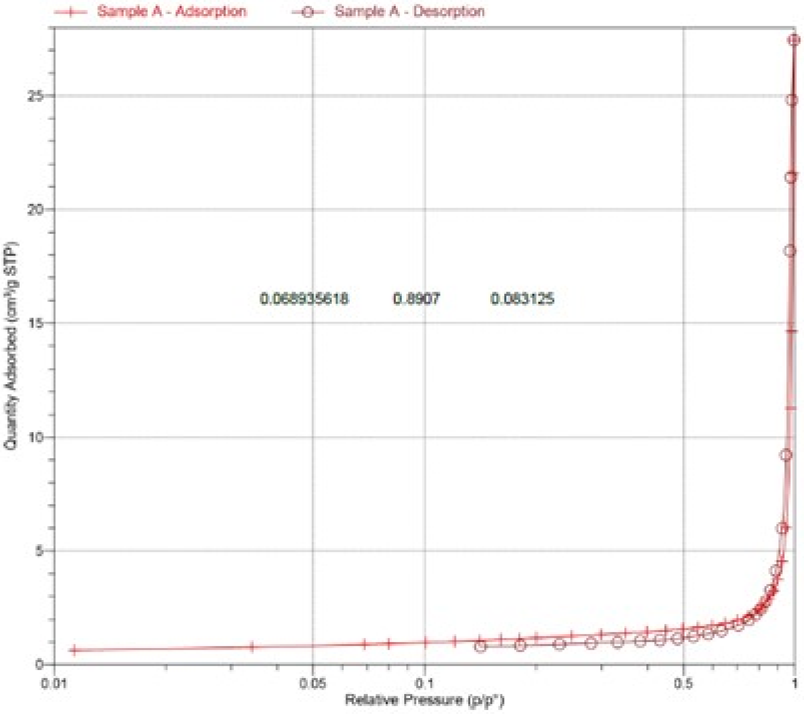

Figure 4. BET isotherms of the Ni-Co/alumina homemade catalyst

3.2 Kinetics of TCD reaction

The present study examined the kinetics of the TCD process over the homemade Ni-Co/alumina catalyst and the Ni/alumina commercial catalyst at different reaction temperatures (800 and 900°C) and mole fractions of methane (0.6-1.0). Figure 5 shows the kinetic profiles of the commercial catalyst at 800°C and different mole fractions of methane. After a reaction time less than 5 min increasing methane mole fraction from 0.6 to 0.7 resulted in a slight increase in methane conversion (18.5 % to 29 %). However, as the mole fraction of methane was increased from 0.7 to 0.8, the conversion was enhanced to 52%, which is a highly significant increase at a short time of reaction (5 min). This increase may attribute to the reduction of mass transfer resistance in the feed gasses mixture as the concentration of methane approaches the critical value of 0.8-mole fraction [26, 35, 36]. For the other examined concentrations at 0.9 and 1.0, the conversion was slightly enhanced to 58 % and 60%. However, after 5 min on stream, it was obvious the increase of TCD conversion was stopped at 0.6 and 0.7 and significantly fell to low values for 0.8 (less than 20%), 0.9 (21.5%), and 1.0 (25.7%).

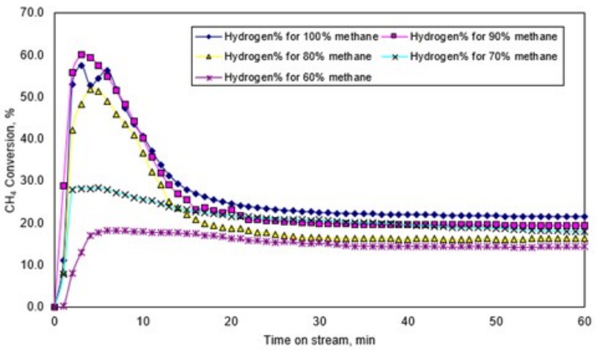

Figure 5. Conversion of methane versus time on stream over the Ni/alumina commercial catalyst at 800 °C and different mole fractions (0.6-1)

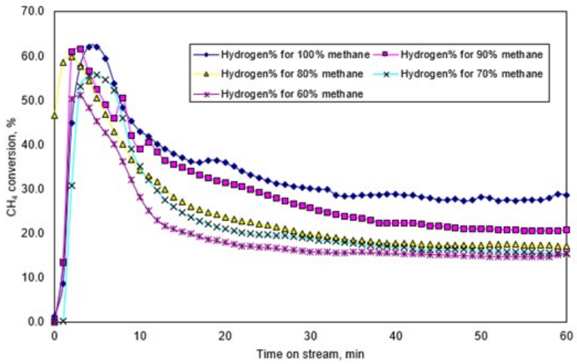

Figure 6. Conversion of methane versus time on stream over the Ni/alumina commercial catalyst at 900 °C and different mole fractions (0.6-1)

The reason behind this obvious fall is due to byproduct carbon deposition on the surface of the commercial catalyst. Thus, the pore volume was shrunk to low volume after a short time of reaction. At 900°C, Figure 6 depicts that the activity of the commercial catalyst for the TCD process was enhanced significantly for the methane mole fractions of 0.6 and 0.7 compared to the activities obtained at 800°C. It can be seen that methane conversion was increased to 51.3% at 4 min on stream and 0.6-mole fraction of methane. The maximum conversions achieved for the other mole fraction were 60%, 61.5, and 63 for 0.8, 0.9, and 1.0, respectively. The conversion was enhanced by the increase in temperature due to the increase in collision energy at higher temperatures [27, 30, 37]. A similar catalyst deficiency was observed for the commercial Ni/alumina catalyst after a short time on stream. Figure 6 shows that the maximum conversions fell to 18%, 19.5%, 21%, 26% and 32 % for 0.6, 0.7, 0.8, 0.9 and 1.0-mole fraction respectively. Like the TCD examined at 800 °C, the deficiency started after a short time on stream due to the same reason of carbon deposition in the catalyst pores at the high temperature of methane decomposition. Also, the rate of deactivation depends on the catalyst characteristics and operating conditions [38], thereby, the observed deactivation may attribute to the formation of a new catalyst active phase promoted by the higher metal (nickel) loading. From these findings, it can be suggested that the initial activity of the commercial catalyst was satisfactory. However, the carbon deposition started rapidly, and the catalyst was deactivated because of catalyst coking and solid phase change.

Figure 7 shows the conversion of methane with time on stream over the homemade Ni-Co/alumina catalyst in the fixed bed reactor at 800°C and different mole fractions of methane (0.6-1.0). The conversion of methane was significantly enhanced and sustained by the co-impregnation of Co with the Ni on the support. In general, Figure 7 depicts that the methane conversion was increased to higher values at all the mole fraction tested compared to the conversion obtained over the commercial catalyst shown in Figure 5. Besides the enhancement in conversion, it is well noticed that the activity of the Ni-Co homemade catalyst was sustained and the conversion continues to rise as time proceeds up to 60 min which is a good indication of the continuity and sustainability of the rate of TCD reaction with time despite the formation of the byproduct carbon. However, at a 0.6-mole fraction of methane, there is a slight deficiency observed after 53 min on stream as the conversion decreases from 41.3% to 38.1 %

at the end of 60 min which is attributes to the consumption of methane as time proceeds and increase of carbon deposited on the surface of the homemade catalyst. A remarkable increase in methane conversion was observed at a mole fraction of 1 as the conversion approached 78.1% and no deactivation was observed up to 60 min on stream compared to 59.3% only achieved with the commercial Ni catalyst at 8 min on stream and fell to 22.8% at the end of test time of 60 min. At the other mole fractions of methane 0.9, 0.8, and 0.7, the same trend of increased conversion and sustainability of catalyst activity was observed; 69.1%, 58.2%, and 43.7%, respectively. For the highest temperature tested on the homemade catalyst, Figure 8 shows the methane conversion profiles with time on stream at 900°C and different mole fractions of methane in a fixed bed reactor.

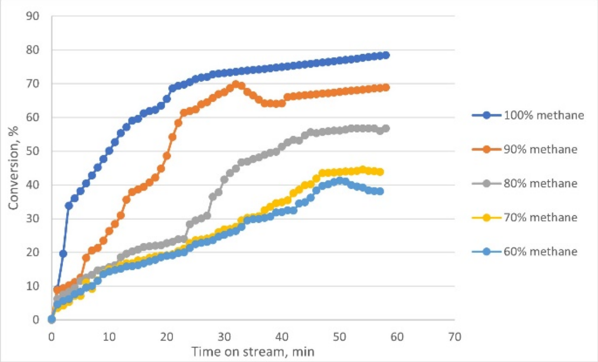

Figure 7. Conversion of methane versus time on stream over the homemade Ni-Co/alumina catalyst at 800 °C and different mole fractions (0.6-1)

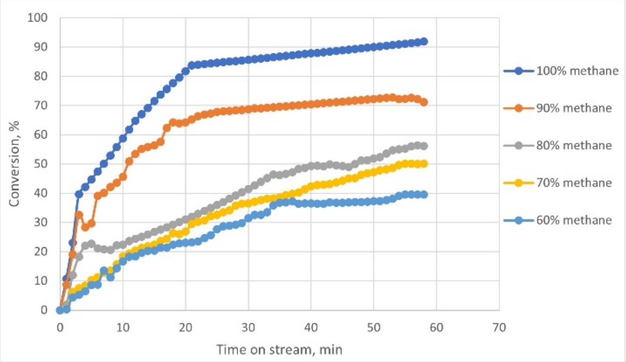

Figure 8. Conversion of methane versus time on stream over the homemade Ni-Co/alumina catalyst at 900 °C and different mole fractions (0.6-1)

An outstanding performance of the prepared Ni-Co catalyst was achieved at 900°C as a noticeable rise in conversion, and remarkable sustainability was depicted by all profiles obtained at 0.6-1.0 mole fraction of methane. The highest conversion achieved at this temperature was 91.8% at a 1.0-mole fraction of methane. This high conversion is not only attributed to the high activity of the prepared catalyst caused by the addition of Co, but it also relates to the forming of new TCD catalysis enhancing material at the time of reaction and a more active solid phase of the catalyst. As time on stream proceeds, there is no significant fall in activity of the catalyst at all the tested mole fractions and 900°C despite the formation of the byproduct carbon. Compared to the conversion achieved via the homemade catalyst at 800°C, the conversions were increased to 71.2%, 56.1%, 50%, and 39.5% for 0.9, 0.8, 0.7, and 0.6 methane mole fractions with no significant deactivation. According to the conversion profiles achieved in Figures 7 and 8, the best operating mole fraction of methane in the TCD process at 800°C and 900°C over the Ni-Co/alumina homemade catalyst is 1.0. Thus, the TCD reaction rate laws were obtained via analysis of the experimental conversion against time according to equation 5 as follow;

At 800°C: $-r_{CH_4} = -\frac{dC_{CH_4}}{dt} = 1.744\ C_{CH_4}^{0.613}$ (7)

At 900°C: $-r_{CH_4} = -\frac{dC_{CH_4}}{dt} = 3.084\ C_{CH_4}^{0.587}$ (8)

The Arrhenius equation parameters K_0 and E_A showed in equation 3 were obtained by plotting ln K_{apps} obtained in equations 6 and 7 versus the reciprocal of TCD temperature in the temperature range of 800°C (1073 K) to 900°C (1173 K) as shown in Figure 9.

Thus, $-\frac{E_A}{R} = -7174.8,\ Take\ R = 8.314\frac{J}{mol.K}, E_A = 8.314 \times 7174.8 = 59.651\ \frac{kJ}{molCH_4}$

and ln K_o= 7.242 gives K_0= 1396.8

3.3. Morphology of byproduct carbon deposited in TCD reaction

It has been shown via results of TCD conversion using the Ni-Co/alumina homemade catalyst that homemade catalyst does not experience a significant deactivation at the time of

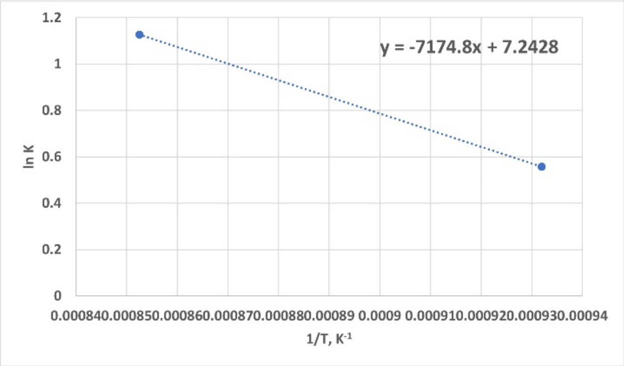

Figure 9. Arrhenius plot for TCD of methane over the Ni-Co homemade catalyst at a 1.0-mole fraction of methane between 800 and 900 °C

testing despite the expected formation of the carbon as a byproduct of the TCD reaction. Therefore, it is worthy of examining the morphology of the spent homemade catalyst under a transmission electron microscope (TEM) to magnify the form of carbon generated at the time of TCD reaction. Figure 10 shows the TEM images of a sample of the spent homemade catalyst under different magnifications. The sample was taken from the catalyst used for the experimental runs implemented at 900°C and the 1.0-mole fraction of methane.

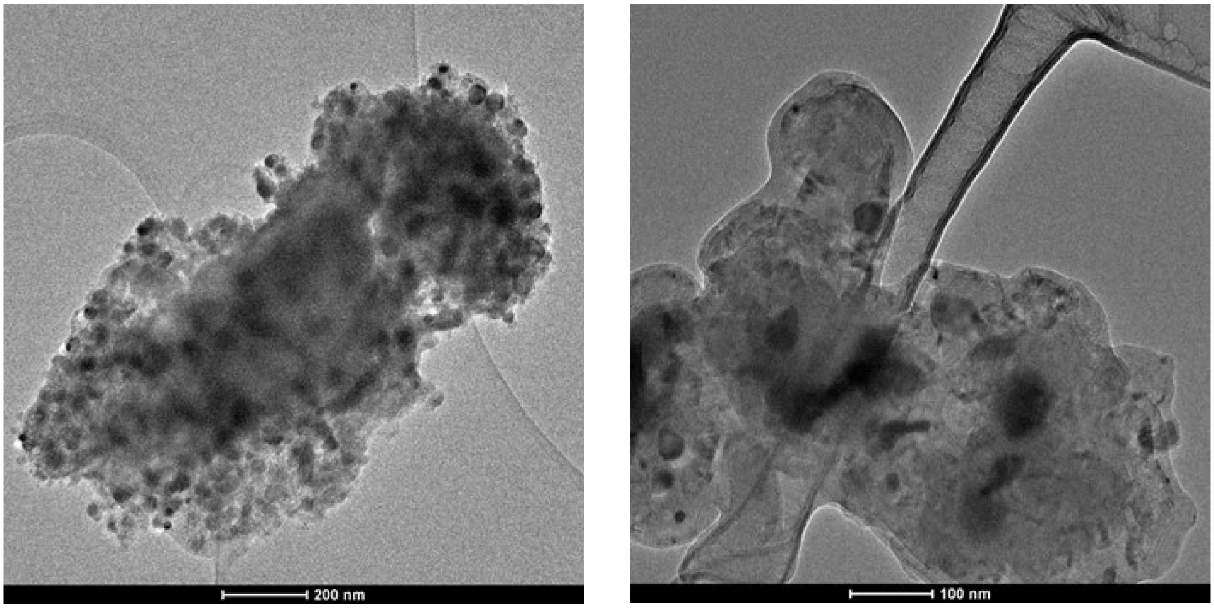

Figure 10. TEM of the spent Ni-Co/alumina homemade catalyst undergoes TCD reaction at 900°C and a 1.0-mole fraction of methane

It is seen that carbon nanotubes were formed on the surface of the catalyst; these tubes were formed along with spherical shape carbon deposits. The generation of these nanotubes is caused by oxygen supplied by the presence of cobalt oxide and resulted in oxidized part of the catalyst along with other reduced parts of the catalyst that provides sufficient energy for the TCD reaction of methane which is endothermic and adsorb some of the carbon and hydrogen needed to generate CO and water. Thus, the equilibrium state of TCD reaction shifts to the direction of producing pure hydrogen along with form carbon nanotubes [36-37]. Then, the carbon nanotubes will provide a high surface area for the production of hydrogen compared to the area provided by the regular carbon in the experiments conducted with the commercial catalyst [39-41]. It is also shown from Figure 10 that the diameter of the carbon nanotube form was about 50 nm, which is larger than other carbon nanotubes obtained in previous studies [5, 41, 42]. In these studies, multiwall and double walls carbon nanotubes and were obtained as a byproduct in the TCD reaction of methane using Ni catalyst promoted by different metals such as Co, Cu, and Mg.

4. Conclusion

For the benign production of hydrogen and carbon nanotubes, which is of several industrial applications, the present study was implemented. Via thermocatalytic decomposition of methane, the production of CO_X free hydrogen, was achieved via the preparation of Ni-Co catalyst by co-impregnation method over gamma-alumina. The characterizations of the prepared catalyst revealed a satisfactory surface area, metal distribution, and pore size. Based on the TCD experiments in the fixed bed reactor, it was found that a more 91% conversion of methane to hydrogen and carbon nanotubes was achieved at 900°C and the 1.0-mole fraction of methane. It was also proven that the prepared catalyst did not experience a deactivation as the time of processing proceeds. The testing of the TCD reaction rate law based on the homemade catalyst showed that the reaction order is less than one, and the activation energy obtained was satisfactory in comparison to previous studies. Upon magnification of the deposited byproduct carbon, it was observed that the carbon deposited was in the form of single-wall carbon nanotube, and this was one of the reasons behind the sustainability of the homemade catalyst developed in the present study.

References

[1] Dowdy TE. Coal gasification and hydrogen production system and method. In: Google Patents; 1999.
[2] Stiegel GJ, Ramezan M. Hydrogen from coal gasification: An economical pathway to a sustainable energy future. International journal of coal geology 2006; 65(3-4): 173-190.
[3] Xiang W, Chen S, Xue Z, Sun X. Investigation of coal gasification hydrogen and electricity co-production plant with three-reactors chemical looping process. International journal of hydrogen energy 2010; 35(16): 8580-8591.
[4] LeValley TL, Richard AR, Fan M. The progress in water gas shift and steam reforming hydrogen production technologies–a review. International Journal of Hydrogen Energy 2014; 39(30): 16983-17000.
[5] Heinzel A, Vogel B, Hübner P. Reforming of natural gas—hydrogen generation for small scale stationary fuel cell systems. Journal of Power Sources 2002; 105(2): 202-207.
[6] Spath PL, Mann MK. Life cycle assessment of hydrogen production via natural gas steam reforming. In: National Renewable Energy Lab., Golden, CO (US); 2000.
[7] Vaidya PD, Rodrigues AE. Insight into steam reforming of ethanol to produce hydrogen for fuel cells. Chemical Engineering Journal 2006; 117(1): 39-49.
[8] Palo DR, Dagle RA, Holladay JD. Methanol steam reforming for hydrogen production. Chemical reviews 2007; 107(10): 3992-4021.
[9] Liguras DK, Kondarides DI, Verykios XE. Production of hydrogen for fuel cells by steam reforming of ethanol over supported noble metal catalysts. Applied Catalysis B: Environmental 2003; 43(4): 345-354.
[10] Yamada O. Generation of hydrogen gas by reforming biomass with superheated steam. Thin solid films 2006; 509(1-2): 207-211.
[11] Magrini-Bair K, Czernik S, French R, Parent Y, Ritland M, Chornet E. Fluidizable catalysts for producing hydrogen by steam reforming biomass pyrolysis liquids. In: Proceedings of the 2002 US DOE Hydrogen Program Review NREL/CP-610; 2002.
[12] Czernik S, Evans R, French R. Hydrogen from biomass-production by steam reforming of biomass pyrolysis oil. Catalysis Today 2007; 129(3-4): 265-268.
[13] Bimbela F, Oliva M, Ruiz J, García L, Arauzo J. Hydrogen production by catalytic steam reforming of acetic acid, a model compound of biomass pyrolysis liquids. Journal of Analytical and Applied Pyrolysis 2007; 79(1-2): 112-120.
[14] Doenitz W, Schmidberger R, Steinheil E, Streicher R. Hydrogen production by high temperature electrolysis of water vapour. International Journal of Hydrogen Energy 1980; 5(1): 55-63.
[15] Rashid MM, Al Mesfer MK, Naseem H, Danish M. Hydrogen production by water electrolysis: a review of alkaline water electrolysis, PEM water electrolysis and high temperature water electrolysis. Int J Eng Adv Technol 2015; 4(3): 2249-8958.
[16] Rossmeisl J, Logadottir A, Nørskov JK. Electrolysis of water on (oxidized) metal surfaces. Chemical physics 2005; 319(1-3): 178-184.
[17] Rossmeisl J, Qu Z-W, Zhu H, Kroes G-J, Nørskov JK. Electrolysis of water on oxide surfaces. Journal of Electroanalytical Chemistry 2007; 607(1-2): 83-89.

[18] Guil-Lopez R, La Parola V, Pena M, Fierro J. Evolution of the Ni-active centres into ex hydrotalcite oxide catalysts during the COx-free hydrogen production by methane decomposition. International journal of hydrogen energy 2012; 37(8): 7042-7055.

[19] Rodríguez-Lugo RE, Trincado M, Vogt M, Tewes F, Santiso-Quinones G, Grützmacher H. A homogeneous transition metal complex for clean hydrogen production from methanol–water mixtures. Nature chemistry 2013; 5(4): 342.

[20] Winter C-J. Hydrogen energy—Abundant, efficient, clean: A debate over the energy-system-of-change. International journal of hydrogen energy 2009; 34(14): S1-S52.

[21] Hosseini SE, Wahid MA. Hydrogen production from renewable and sustainable energy resources: promising green energy carrier for clean development. Renewable and Sustainable Energy Reviews 2016; 57: 850-866.

[22] Kothari R, Singh D, Tyagi V, Tyagi S. Fermentative hydrogen production–An alternative clean energy source. Renewable and Sustainable Energy Reviews 2012; 16(4): 2337-2346.

[23] Naterer G, Suppiah S, Stolberg L, Lewis M, Ferrandon M, Wang Z, Dincer I, Gabriel K, Rosen MA, Secnik E, Easton EB, Trevani L, Pioro I, Tremaine P, Lvov S, Jiang J, Rizvi G, Ikeda BM, Lu L, Kaye M, Smith WR, Mostaghimi J, Spekkens P, M Fowler, Avsec J. Clean hydrogen production with the Cu–Cl cycle–progress of international consortium, I: experimental unit operations. International Journal of Hydrogen Energy 2011; 36(24): 15472-15485.

[24] Srinivas G, Ford J, Zhou W, Yildirim T. Zn-MOF assisted dehydrogenation of ammonia borane: enhanced kinetics and clean hydrogen generation. international journal of hydrogen energy 2012; 37(4):3633-3638.

[25] Takenaka S, Kobayashi S, Ogihara H, Otsuka K. Ni/SiO_2 catalyst effective for methane decomposition into hydrogen and carbon nanofiber. Journal of catalysis 2003; 217(1): 79-87.

[26] Kim MH, Lee EK, Jun JH, Kong SJ, Han GY, Lee BK, Lee T-J, Yoon KJ. Hydrogen production by catalytic decomposition of methane over activated carbons: kinetic study. International journal of hydrogen energy 2004; 29(2): 187-193.

[27] Pinilla J, Utrilla R, Karn R, Suelves I, Lázaro M, Moliner R, Garcia AB, Rouzaud J-N. High temperature iron-based catalysts for hydrogen and nanostructured carbon production by methane decomposition. International Journal of hydrogen energy 2011; 36(13): 7832-7843.

[28] Li Y, Li D, Wang G. Methane decomposition to COx-free hydrogen and nano-carbon material on group 8–10 base metal catalysts: a review. Catalysis today 2011; 162(1):1-48.

[29] Bayat N, Rezaei M, Meshkani F. Methane decomposition over Ni–Fe/Al_2O_3 catalysts for production of COx-free hydrogen and carbon nanofiber. International journal of hydrogen energy 2016; 41(3):1574-1584.

[30] Pudukudy M, Yaakob Z, Takriff MS. Methane decomposition over Pd promoted Ni/$MgAl_2O_4$ catalysts for the production of COx free hydrogen and multiwalled carbon nanotubes. Applied Surface Science 2015; 356: 1320-1326.

[31] Li D, Chen J, Li Y. Evidence of composition deviation of metal particles of a Ni–Cu/Al_2O_3 catalyst during methane decomposition to COx-free hydrogen. international journal of hydrogen energy 2009; 34(1): 299-307.

[32] Awadallah A, Ahmed W, El-Din MN, Aboul-Enein A. Novel aluminosilicate hollow sphere as a catalyst support for methane decomposition to COx-free hydrogen production. Applied surface science 2013; 287: 415-422.

[33] Pudukudy M, Yaakob Z, Mazuki MZ, Takriff MS, Jahaya SS. One-pot sol-gel synthesis of MgO nanoparticles supported nickel and iron catalysts for undiluted methane decomposition into COx free hydrogen and nanocarbon. Applied Catalysis B: Environmental 2017; 218:298-316.

[34] Al-Fatesh A, Fakeeha A. Effects of calcination and activation temperature on dry reforming catalysts. Journal of Saudi Chemical Society 2012; 16(1):55-61.

[35] Piao L, Li Y, Chen J, Chang L, Lin JY. Methane decomposition to carbon nanotubes and hydrogen on an alumina supported nickel aerogel catalyst. Catalysis Today 2002; 74(1-2): 145-155.

[36] Qian W, Liu T, Wei F, Wang Z, Li Y. Enhanced production of carbon nanotubes: combination of catalyst reduction and methane decomposition. Applied Catalysis A: General 2004; 258(1): 121-124.

[37] Takenaka S, Ishida M, Serizawa M, Tanabe E, Otsuka K. Formation of carbon nanofibers and carbon nanotubes through methane decomposition over supported cobalt catalysts. The Journal of Physical Chemistry B 2004; 108(31): 11464-11472.

[38] Makvandi S, Alavi S. COx free hydrogen production by catalytic decomposition of methane over porous Ni/Al_2O_3 catalysts. Iranian Journal of Chemical Engineering, 2011; 8: 24–33 .

[39] He C, Zhao N, Shi C, Du X, Li J. Carbon nanotubes and onions from methane decomposition using Ni/Al catalysts. Materials chemistry and physics 2006; 97(1): 109-115.

[40] Chai S-P, Zein SHS, Mohamed AR. Preparation of carbon nanotubes over cobalt-containing catalysts via catalytic decomposition of methane. Chemical Physics Letters 2006; 426(4-6):345-350.

[41] Chai S-P, Zein SHS, Mohamed AR. The effect of catalyst calcination temperature on the diameter of carbon nanotubes synthesized by the decomposition of methane. Carbon 2007; 45(7): 1535-1541.

[42] Benito P, Herrero M, Labajos F, Rives V, Royo C, Latorre N, Monzon A. Production of carbon nanotubes from methane: use of Co-Zn-Al catalysts prepared by microwave-assisted synthesis. Chemical Engineering Journal 2009; 149(1-3): 455-462.

To whom correspondence should be addressed: Hiba A. Abdulkareem, Department of Petroleum Processes, Tikrit University, Iraq, E-mail: cssuiq@gmail.com